J Mater Sci (2018) 53:10653–10665

Biomaterials

Dual-pH-sensitive mesoporous silica nanoparticle-based drug delivery system for tumor-triggered intracellular drug release

Hui Chen[1], Ying Kuang[2], Rong Liu[1], Zhongyin Chen[1], Bingbing Jiang[1], Zhengguang Sun[1], Xueqin Chen[1,*], and Cao Li[1,*]

[1] *Hubei Collaborative Innovation Center for Advanced Organic Chemical Materials, Key Laboratory for the Green Preparation and Application of Functional Materials of Ministry of Education, Hubei University, Wuhan 430062, Hubei, People's Republic of China*

[2] *Glyn O. Philips Hydrocolloid Research Centre at HUT, Hubei University of Technology, Wuhan 430068, Hubei, People's Republic of China*

Received: 29 January 2018
Accepted: 23 April 2018
Published online: 8 May 2018

ABSTRACT

Reducing the side effects and improving the drug utilization are important work in anti-cancer drug delivery. In this paper, a novel dual-pH-sensitive drug delivery system was reported. Mesoporous silica nanoparticle (MSN) was applied to load anti-cancer drug doxorubicin hydrochloride (DOX) and was covered by mono-6-deoxy-6-EDA-β-cyclodextrine (β-CD-NH_2) to block the pores through pH-sensitive boronate ester bond. And the carriers were then coated with methoxy poly(ethylene glycol) (mPEG) through another pH-sensitive benzoic imine bond. mPEG leaving studies, in vitro cellular uptake studies and the flow cytometry analysis, proved that carriers was "stealthy" at pH 7.4, but could be "activated" for cytophagy by cancer cells in weakly acidic tumor tissues (pH 6.5) due to the departure of mPEG. β-CD-NH_2 leaving studies, the in vitro drug release studies and the in vitro cytotoxicity studies proved that boronate ester bond linking MSN and β-CD-NH_2 was stable at both pH 7.4 and 6.5, but could be hydrolyzed intracellular to release DOX for cellular apoptosis due to the lower pH (5.0). In summary, the novel dual-pH-sensitive drug delivery system fabricated with a dynamic protection strategy should have great application potential in anti-cancer drug delivery fields.

Introduction

Excellent anti-cancer drug delivery systems (DDSs) should be safe and have long circulation time in blood, could be accumulated and penetrate into tumor for cellular internalization, and at last could release the drug intracellular [1, 2]. Therefore, the biocompatibility, safety, targeted property and controlled released behavior as well as the property of being "stealthy" in blood and normal tissues but

Address correspondence to E-mail: chenxueqin@hubu.edu.cn; licao0415@163.com

https://doi.org/10.1007/s10853-018-2363-8

being "activated" to stick the cancer cells are profoundly significant for outstanding DDSs [1–6]. Among the well-studied DDSs such as liposomes [7, 8], micelles [9], vesicles [8], inorganic nanoparticles [10], mesoporous silica nanoparticle (MSN)-based DDSs are valuable choices [11, 12]. Due to the advantages such as good biocompatibility and low toxicity, high drug loading capacity, suitable size with an enhanced permeation and retention (EPR) property, excellent chemical stability and well-studied surface functionalization, MSNs have been widely researched as advanced DDSs [11–14].

For most of the reported works, MSNs were capped with gatekeepers who could respond to different stimuli for controlled drug release [13, 14]. Due to the differences between the microenvironments of normal tissues and tumor tissues, and the differences between the extracellular matrix (ECM) and environments intracellular, various stimuli such as temperature [15], pH [16], enzyme [17], redox potential [18] have been utilized to design intelligent MSN-based DDSs as well as artificial stimuli such as light [19], irradiation [20], ultrasound [21] and so on. The strategies of stimuli-response reduce the premature drug release from the DDSs in blood and normal tissues effectively [14, 21]. However, without appropriate protection, the drug carriers may easily aggregate and be rapid cleared during the circulation or be unspecific uptake by normal cells due to the complicated environments in vivo, which may reduce the utilization of the drugs [22]. Therefore, dynamic protection strategy is an effective supplement of traditional MSN-based DDSs [18]. "Stealthy" polymers such as poly(ethylene glycol) (PEG) and polyanions can inhibit nonspecific interaction of drug carriers with serum proteins and normal tissues [23, 24]; however, they can also diminish the cellular uptake by cancer cells [25]. As a result, by introducing the dynamic protection strategy, e.g., coating of PEG on the surface of DDSs through dynamic chemical bonds which are stable in bloodstream and normal tissues but can be disconnected in tumor tissues, can assure the carriers being "stealthy" before they reach the tumor tissues and being "activated" due to the microenvironments of tumor tissues [18, 26]. One of the most important dynamic chemical bonds applied is benzoic imine bond [27]. Benzoic imine bond is formed from amino group and benzaldehyde, and is stable at pH 7.4, but can be easily hydrolyzed in weakly acidic environments [18, 26, 27]. The tumor extracellular environment is slightly acidic ($pH_e < 6.8$) [28]; therefore, benzoic imine bond is stable in bloodstream and normal tissues (pH 7.4), but can be hydrolyzed at pH_e [18, 26, 27]. After being grafted with PEG through benzoic imine bond on the surface of the drug carriers, scientists could endow the carriers with the property of tumor-triggered targeting or tumor-triggered intracellular drug release [18, 26, 28, 29].

In this work, based on dynamic protection strategy, we report a dual-pH-sensitive MSN-based DDS named DOX@MSN-B-CD-PEG for tumor-triggered intracellular drug release. As shown in Scheme 1, the doxorubicin hydrochloride (DOX)-loaded drug carriers were grafted with methoxy PEG (mPEG) through benzoic imine bond, to make which "stealthy" before they reach the tumor tissues. Inside the mPEG shield, MSN was capped with mono-6-deoxy-6-EDA-β-cyclodextrin (β-CD-NH_2) via another pH-sensitive linker boronate ester bond. Though pH_e of tumor tissue is slightly lower than 7.4, the pH intracellular (pH_i) is even lower (4.5–6.5) [28, 30]. Boronate ester bond is formed from diol group and phenylboronic acid. At pH_e, boronate ester bond is stable; however, it can be quickly hydrolyzed at pH 5.0 [31]. Therefore, β-CD-NH_2 could cover the pores of MSN to prevent premature DOX release in bloodstream and normal tissues, and even ECM of tumor tissues. After arriving at the tumor tissues, mPEG could leave the nanoparticles at pH_e, revealing the positive-charged amino groups, which could enhance the cellular uptake of the carriers. The hydrolysis of boronate ester bond at pH_i could lead to the opening of β-CD cap and releasing the DOX to kill the cancer cells. With the dynamic protection strategy and dual-pH-sensitivity, DOX@MSN-B-CD-PEG could achieve the purpose of tumor-triggered intracellular drug release and should be an effective choice for anticancer drug delivery.

Experimental section

Chemicals

Tetraethylorthosilicate (TEOS), *N*-cetyltrimethylammonium bromide (CTAB), NaOH, hydrochloric acid (HCl), β-cyclodextrin (β-CD), *p*-toluenesulfonyl chloride (*p*-TsCl), ethylenediamine (EDA), triethylamine, NH_4Cl, Na_2SO_4, acetone and anhydrous methanol

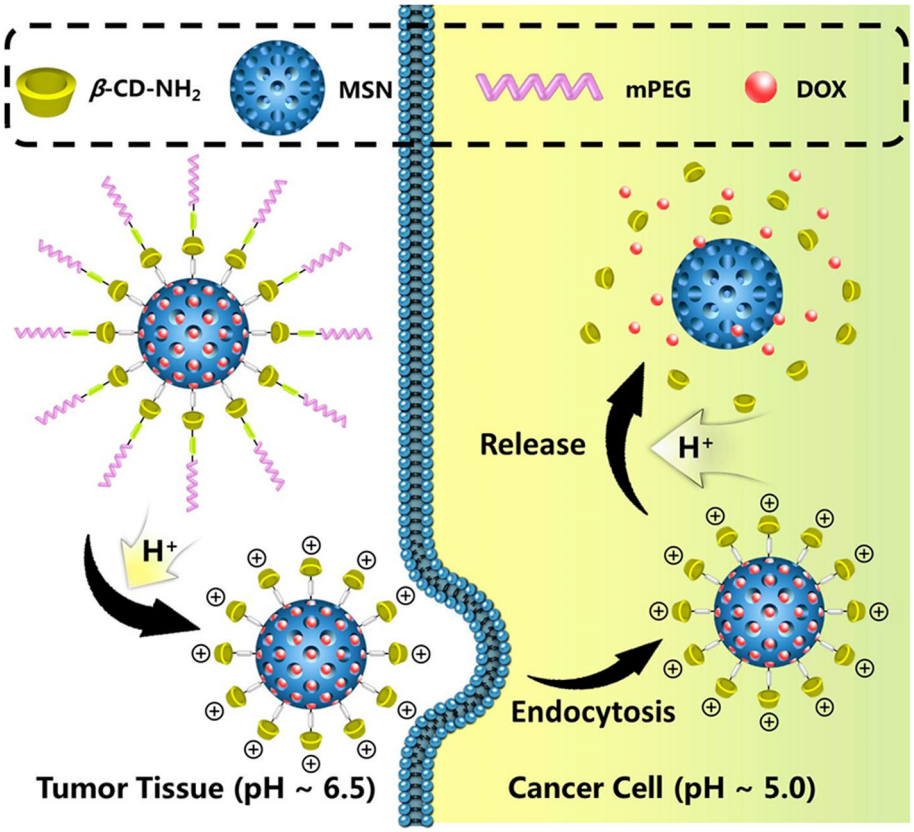

Scheme 1 Schematic design of the tumor-triggered intracellular drug release process of DOX@MSN-B-CD-PEG.

were purchased from Shanghai Reagent Chemical Co. (Shanghai, China). (3-aminopropyl)triethoxysilane (APTES), mPEG (M_w = 1900 Da), 4-formylbenzoic acid, 3-(bromomethyl)phenylboronic acid, 4-dimethylaminopyridine (DMAP), *N*,*N*′-dicyclohexylcarbodiimide (DCC) and DOX were purchased from Aladdin Reagent Co. Ltd. (Shanghai, China). Phosphate-buffered saline (PBS), Dulbecco's modified eagle medium (DMEM), fetal bovine serum, (FBS) 3-[4,5-dimethylthiazol-2-yl]-2,5-diphenyltetrazolium-bromide (MTT) and DAPI were purchased from Invitrogen Co. (America). All reagents were of analytical grade and were used as received. The syntheses of methoxy poly(ethylene glycol) benzaldehyde (mPEG-CHO) and β-CD-NH_2 are shown in the Supplementary data.

Preparation of DOX@MSN-B-CD-PEG

The preparation of MSN and amine functionalized MSN (MSN-NH_2) was followed a reference procedure and are shown in the Supplementary data [32]. MSN-NH_2 (0.6 g) was well dispersed in methanol (120 mL). Then, 3-(bromomethyl)phenylboronic acid (1.0 g) was added to the suspension with two drops of triethylamine. The mixture was refluxed at 70 °C for 24 h. The white powder was centrifuged and washed with methanol and dried under vacuum to obtain benzoboric acid functionalized MSN (MSN-$B(OH)_2$).

MSN-$B(OH)_2$ (200 mg) was well dispersed in PBS (100 mL, pH 7.4). Then, DOX (100 mg) was added to the suspension. The mixture was stirred vigorously in dark at 40 °C for 24 h. After that, β-CD-NH_2 (200 mg) was added to the suspension. The reaction was continued in dark at 40 °C for 24 h. The white powder was centrifuged and washed with deionized (DI) water, and lyophilized to obtain DOX loaded β-CD-NH_2 capped MSN (DOX@MSN-B-CD-NH_2).

DOX@MSN-B-CD-NH_2 (200 mg) was well dispersed in PBS (60 mL, pH 7.4). Then mPEG-CHO (200 mg) was added to the suspension. The mixture was stirred at room temperature for 24 h. Then, the white powder was centrifuged and washed with DI water, and dried under vacuum to obtain DOX@MSN-B-CD-PEG. We also synthetized MSN-B-CD-NH_2 and MSN-B-CD-PEG without loading of DOX in the similar way. The drug entrapment

efficiency (EE) and the drug loading capacity (LC) of the drug carriers were calculated based on the following equations:

$$EE = \frac{\text{mass of drug loaded in MSN}}{\text{mass of drug fed initially}} \times 100\%$$

$$LC = \frac{\text{mass of drug loaded in MSN}}{\text{mass of drug loaded nanoparticles}} \times 100\%$$

Characterizations

The morphologies of MSN and DOX@MSN-B-CD-PEG were observed by a transmission electron microscope (TEM; Tecnai G20, FEI, USA). Data of particle sizes and zeta-potentials were obtained by a Zetasizer Nano ZS90 analyzer (Malvern, UK). Fourier transform infrared (FT-IR) spectra of all the samples were recorded on a Nicolet iS10 spectrometer (Thermo Fisher, USA). Specific surface area, pore volume, and pore size of all the samples were determined by nitrogen gas adsorption/desorption isotherm calculated by the Brunauer–Emmett–Teller (BET) method and Barrett-Joyner-Halenda (BJH) approach (JW-BK112, Beijing JWGB, China). Thermogravimetric analysis (TGA) was performed from 30 to 800 °C at heating rate of 5 °C/min under N_2 atmosphere with a TGA/DSC 1-1100c analyzer (Mettler Toledo, Sweden). UV–Vis spectra were obtained using a Lambda Bio40 UV/Vis spectrometer (PerkinElmer, USA).

pH_e-dependent mPEG leaving and pH_i-dependent β-CD-NH_2 leaving studies

The pH_e-dependent mPEG leaving and pH_i-dependent β-CD-NH_2 leaving studies were taken at pH 7.4, 6.5 and 5.0, respectively, which were chosen to imitate the neutral environments of normal tissues, the weakly acidic environments of tumor tissues and the acidic environments intracellular. For each study, DOX@MSN-B-CD-PEG was suspended and shaken in buffer solution at 37 °C. Then, the nanoparticles were centrifuged to withdraw from the solution periodically. The obtained nanoparticles were washed with DI water for three times and were suspended in DI water for the zeta-potential measurements to observe the mPEG leaving and β-CD-NH_2 leaving behavior of the carriers.

pH_i-dependent in vitro release studies

The in vitro release experiments were performed at 37 °C in buffer solutions at pH 7.4, 6.5 and 5.0, respectively. For each study, DOX@MSN-B-CD-PEG (3.0 mg) was suspended in with the indicated pH buffer solution (5.0 mL) in a dialysis tube, which was immediately immersed into the indicated buffer solution (25.0 mL) and was shaken in a water bath at 37 °C. Samples (4.0 mL) were drawn periodically and replaced with an equal volume of buffer solution. The amount of drug released was calculated based on the UV–Vis absorbance of DOX at 493 nm.

pH_e-dependent in vitro cellular uptake studies

Human cervix carcinoma (HeLa) cells were seeded in a six-well plate at a density of $\sim 1 \times 10^5$ cells per well in DMEM medium with 10% FBS (1 mL), and were incubated (37 °C and 5% CO_2) for 24 h. After that, the culture media was removed and replaced with DMEM containing DOX@MSN-B-CD-PEG with a DOX concentration of 2 mg/L (1 mL) at pH 7.4 and 6.5, respectively. The cells were incubated for a further 4 h. Then the culture medium was removed, and the cells were washed with PBS for three times. After that, the nucleuses were stained with by 500 μL DMEM containing 50 μL of DAPI for 20 min. Finally, the culture medium was removed and the cells were further washed with PBS for several times. Then, the cells were observed by a confocal laser scanning microscopy (CLSM, Nikon C1si, Japan).

Flow cytometry analysis

HeLa cells were seeded in a six-well plate at a density of $\sim 1 \times 10^5$ cells per well in DMEM medium with 10% FBS (1 mL) and were incubated (37 °C and 5% CO_2) for 24 h. After that, the culture media was removed and replaced with DMEM containing DOX@MSN-B-CD-PEG with a DOX concentration of 2 mg/L (1 mL) at pH 7.4 and 6.5, respectively. The cells were incubated for a further 4 h. Then, the culture medium was removed, and the cells were washed with PBS for three times. All the cells were digested by trypsin and collected in centrifuge tubes by centrifugation (1000 rpm for 5 min). The supernatant was discarded, and the bottom cells were washed twice with PBS (pH 7.4). Then, the

suspended cells were filtrated and examined by flow cytometry. Cells untreated with nanoparticles were used as a control.

In vitro cytotoxicity assay

HeLa cells were seeded in a 96-well plate at a density of $\sim 5.0 \times 10^4$ cells per well in DMEM medium with 10% FBS (100 μL) for 24 h to adding pure MSN-B-CD-PEG (without loading of DOX) at different concentrations. After *co*-incubation with the nanoparticles for 48 h, the culture media were replaced with fresh DMEM (200 μL) and MTT stock solution (20 μL, 5 mg/mL in PBS). The cells were incubated for a further 4 h. After that, the culture medium was removed and 200 μL of DMSO was added. The optical density (OD) at 570 nm was measured using a microplate reader (Model 550, Bio-Rad, USA), and the viability was calculated as follows:

$$\text{Cell viability} = \frac{\text{OD}_{570(\text{treated})}}{\text{OD}_{570(\text{control})}} \times 100\%$$

where $\text{OD}_{570(\text{treated})}$ was obtained in the presence of the nanoparticles.

For the cell death assay of DOX loaded DOX@MSN-B-CD-PEG at indicated pH values (7.4 and 6.5, respectively), the cells were seeded in a 96-well plate in DMEM containing 10% FBS (200 μL). After incubation for 24 h, the culture media was replaced with fresh culture media (200 μL) containing DOX@MSN-B-CD-PEG or pure DOX at the indicated DOX concentrations. Somewhat differently, the pH of some of the wells was 7.4 and the pH of others was 6.5. For the wells at pH 6.5, half of which were added with NH_4Cl (20 mM) during the incubation. After *co*-incubation for 48 h, the cell viability was calculated followed the method mentioned above.

Statistical analysis

The results of mPEG leaving studies, in vitro release studies and in vitro cytotoxicity assay were exhibited as mean ± standard deviation (SD) with at least three tests. Statistical significance in difference was analyzed using student's *T* test: $^*p < 0.05$, $^{**}p < 0.01$ and $^{***}p < 0.001$.

Results and discussion

Preparation and characterization of the dual-pH-sensitive drug delivery system

The synthetic process of the dual-pH-sensitive DOX loaded DDS named DOX@MSN-B-CD-PEG was summarized in Scheme 2. Firstly, MSN was synthesized through a base catalyzed sol–gel process and was then reacted with APTES and 3-(bromomethyl)phenylboronic acid successively to obtain MSN-$B(OH)_2$. After loading of DOX, β-CD-NH_2 was introduced to cover the pores through pH-sensitive boronate ester bond. mPEG-CHO was finally grafted outside of the particles via another pH-sensitive bond (benzoic imine) to obtain DOX@MSN-B-CD-PEG.

The geometries of MSN and DOX@MSN-B-CD-PEG were observed by TEM. As shown in Fig. 1a, b, MSNs are regular discrete and spherical particles with highly ordered hexagonal lattice nanoholes. The average diameter of the nanoparticles measured through dynamic light scattering (DLS) was about 175 nm with a PDI of 0.185, which was consistent with that of TEM images (Fig. S3). After the surface functionalization, the hexagonal lattice channels of the MSNs disappeared and the TEM image is shown in Fig. 1c. The phenomenon demonstrated that MSN was covered with organic components.

To confirm the functionalization process of the nanoparticles, zeta-potential measurements, BET method, BJH approach, FT-IR and TGA were employed to characterize the fabrication process of DOX@MSN-B-CD-PEG step by step. As summarized in Table 1, zeta-potential of MSN was measured as − 30.8 mV. After surface modification with APTES, the zeta-potential of MSN-NH_2 reversed to positive of + 44.7 mV due to the amino groups. Then, the surface of the nanoparticles was covered with phenylboronic acid groups; therefore, the zeta-potential reduced to − 8.69 mV. After capped with β-CD-NH_2, the zeta-potential of DOX@MSN-B-CD-NH_2 reversed to positive of + 38.2 mV again. Finally, zeta-potential of DOX@MSN-B-CD-PEG reduced to − 1.33 mV, nearly neutral, as the positive charge of the amino groups was screened by the grafted mPEG.

Figure S4 shows the N_2 adsorption–sorption isotherms and the pore diameter distribution curves of MSN, MSN-NH_2, MSN-$B(OH)_2$, DOX@MSN-B-CD-NH_2 and DOX@MSN-B-CD-PEG, and the data of the BET surface areas (S_{BET}), BJH pore volumes (V_p) and

Scheme 2 Fabrication rout of DOX@MSN-B-CD-PEG.

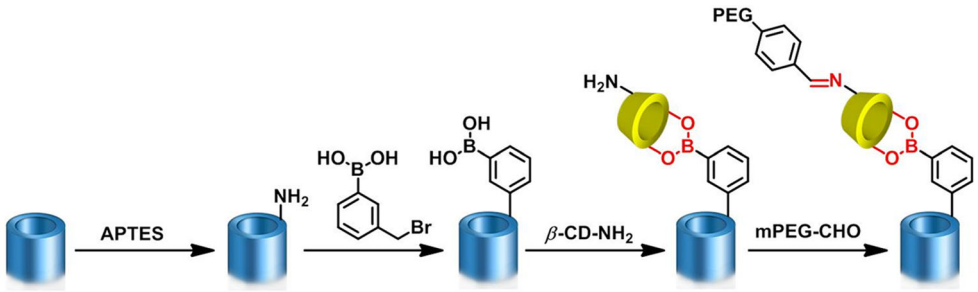

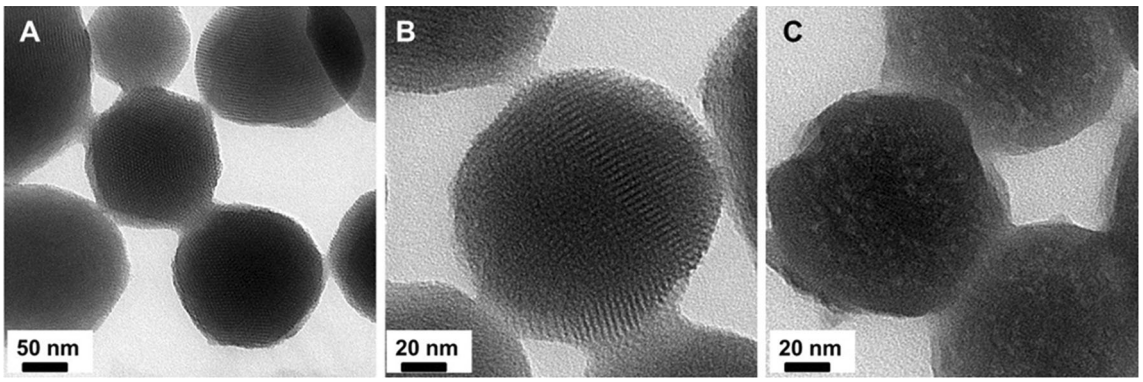

Figure 1 TEM images of MSN (**a** and **b**) and DOX@MSN-B-CD-PEG (**c**).

Table 1 S_{BET}, V_p, D_{BJH} and zeta-potentials of MSN, MSN-NH_2, MSN-$B(OH)_2$, DOX@MSN-B-CD-NH_2 and DOX@MSN-B-CD-PEG

Sample	S_{BET} (m^2/g)	V_p (cm^3/g)	D_{BJH} (nm)	Zeta-potential (mV)
MSN	1169	1.263	3.37	− 30.8
MSN-NH_2	931.4	0.886	3.02	+ 44.7
MSN-$B(OH)_2$	850.0	0.834	2.96	− 8.69
DOX@MSN-B-CD-NH_2	99.47	0.176	–	+ 38.2
DOX@MSN-B-CD-PEG	24.04	0.086	–	− 1.33

BJH pore diameters (D_{BJH}) of all the prepared samples are listed in Table 1 as well. In Fig. S4A, the type IV isotherm curves proved that MSN, MSN-NH_2 and MSN-$B(OH)_2$ owned a typical mesoporous structure. After every modification steps, the adsorption capacity of the nanoparticles reduced gradually, indicated that the pores of the MSN were capped stepwise. For DOX@MSN-B-CD-NH_2 and DOX@MSN-B-CD-PEG, the adsorption capacity reduced obviously, and no clear type IV isotherm curve could be observed, proved that the pores might be totally capped by β-CD. Data of S_{BET}, V_p and D_{BJH} of the samples are in agreement with the curves in Fig. S4. S_{BET} decreased from 1169 m^2/g for MSN to 850.0 m^2/g for MSN-$B(OH)_2$ while V_p decreased from 1.263 to 0.834 cm^3/g stepwise. The pore sizes of MSN, MSN-NH_2 and MSN-$B(OH)_2$ were also slight consecutive reduced from 3.37 nm to 2.96 nm. After being coated with β-CD-NH_2, both S_{BET} and V_p of DOX@MSN-B-CD-NH_2 and DOX@MSN-B-CD-PEG reduced sharply compared with that of MSN-$B(OH)_2$, and D_{BJH} of both nanoparticles could not be calculated, demonstrated the successful surface modification of the MSN as well as that the pores of the nanoparticles had been completely blocked by β-CD-NH_2.

The FT-IR spectra of MSN and all the modified MSNs are exhibited in Fig. 2. The stretching vibration peaks of Si–O–Si near 1080 cm^{-1} and Si–OH near 809 cm^{-1} were existed in all the spectra. After being modified with APTES, the weak bending vibration absorption of –NH_2 appeared at around 1502 cm^{-1} (Fig. 2b), indicated the successful synthesis of MSN-NH_2. Compared with the spectrum of MSN-NH_2, typical absorption peak of –NH_2 disappeared in the spectrum of MSN-$B(OH)_2$ with the stretching

vibration peaks of –B–O– at around 1384 cm^{-1} existed, demonstrated –NH_2 was completely reacted. The FT-IR spectrum of DOX@MSN-B-CD-NH_2 is shown in Fig. 2d. The stretching vibration peak of –CH_2– in β-CD at around 1412 cm^{-1} proved that β-CD-NH_2 had been successfully modified on the nanoparticles. At last, for DOX@MSN-B-CD-PEG, new peaks of PEG at around 3419 cm^{-1} and 2929 cm^{-1} and weak stretching vibration absorption of benzoic imine at around 1651 cm^{-1} proved that the carriers had been coated with mPEG via pH-sensitive benzoic imine bond successfully.

MSN-B-CD-NH_2 and MSN-B-CD-PEG without loading of DOX were also prepared. And the TGA measurements of MSN, MSN-NH_2, MSN-B$(OH)_2$, MSN-B-CD-NH_2 and MSN-B-CD-PEG were taken, respectively. Figure 3 displays the TGA curves of the prepared samples listed above. It is calculated from the TGA data that the weight loss values of MSN, MSN-NH_2, MSN-B$(OH)_2$, MSN-B-CD-NH_2 and MSN-B-CD-PEG at 800 °C were 11.8, 20.6, 25.2, 30.8 and 38.6%, respectively. Compared with MSN, the ratio of the weights of the organic components added to MSN-NH_2 and MSN-B$(OH)_2$ was ~ 1.6:1. And about 38.4% of the amino groups on MSN-NH_2 were substituted by 3-(bromomethyl)phenylboronic acid. It could also be calculated from the TGA data that the molecular number ratio of 3-(bromomethyl)phenylboronic acid and β-CD-NH_2 grafted on the surface of the nanoparticles was ~ 1:0.16. And 93.6% of β-CD-NH_2 was covered with mPEG. Though the ratio of 3-(bromomethyl)phenylboronic acid and β-CD-NH_2 grafted were not high enough; however, the significantly reduced S_{BET} and V_p of DOX@MSN-B-CD-NH_2 and DOX@MSN-B-CD-PEG proved that the large-sized β-CD could block the pores of MSN well. The stepwise increasing of the weight loss values at 800 °C of the samples during the preparation process also proved the successful synthesis of the nanoparticles.

The average diameter of DOX@MSN-B-CD-PEG was also measured and was about 292 nm with PDI of 0.212 (Fig. S3B). The stability of the nanoparticles at pH 7.4 & 37 °C was also studied by dipping the carriers into PBS and measuring the size changes of the nanoparticles. As shown in Fig. S5, the size of DOX@MSN-B-CD-PEG kept in the range of 292–337 nm during the dipping time of 48 h; and no obvious size increasing was observed. The results proved the well stability of the carriers in pH 7.4 PBS.

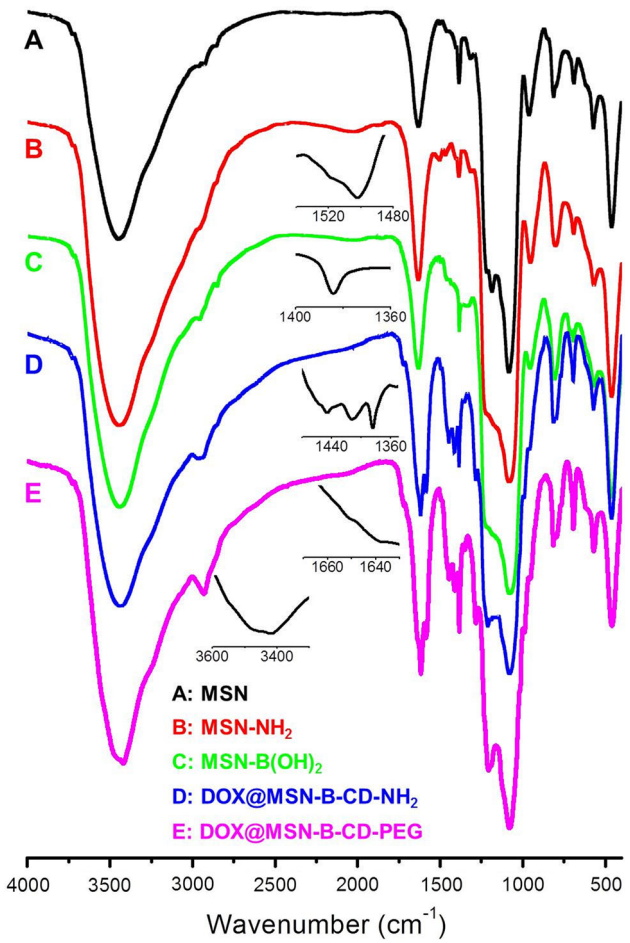

Figure 2 FT-IR spectra of MSN (*a*), MSN-NH_2 (*b*), MSN-B$(OH)_2$ (*c*), DOX@MSN-B-CD-NH_2 (*d*) and DOX@MSN-B-CD-PEG (*e*).

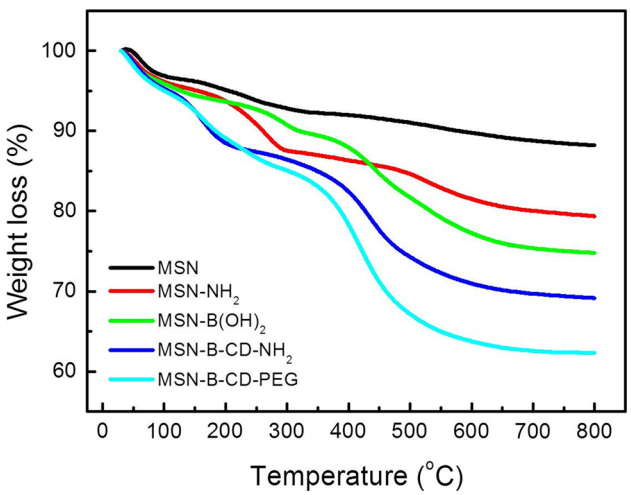

Figure 3 TGA curves of MSN, MSN-NH_2, MSN-B$(OH)_2$, MSN-B-CD-NH_2 and MSN-B-CD-PEG.

pH_e-dependent mPEG leaving and pH_i-dependent β-CD-NH_2 leaving

After being coated with the low protein absorption mPEG, the positive surface charge of DOX@MSN-B-CD-PEG had been shielded; this ensured the "stealthy" property of the drug carriers. To "achieve" the drug carriers to convert for cellular uptake, the mPEG should depart from the nanoparticles due to the low pH in the extracellular matrix (pH_e) of tumor tissues. The mPEG leaving studies were taken through zeta-potential measurements. DOX@MSN-B-CD-PEG was dipped in PBS at pH 7.4 and 6.5 at 37 °C with violent vibration for different times, respectively, and the zeta-potentials of which are shown in Fig. 4. For pH 7.4, the zeta-potentials of the nanoparticles kept at electric neutrality during the dipping process at 48 h (− 0.65 to + 0.58 mV). By contrast, at pH 6.5 (pH_e in tumor tissues), the zeta-potentials of DOX@MSN-B-CD-PEG rose visibly, rose to +10.8 mV within 0.5 h and kept rising to as high as + 36.1 mV within 48 h, approached that of DOX@MSN-B-CD-NH_2 (+ 38.2 mV; Table 1). The results proved that the benzoic imine bonds connecting the nanoparticles and mPEG was steady at pH 7.4 and could be disconnected in weakly acidic environments (pH_e ~ 6.5). That was, the drug carriers should be "stealthy" in blood and normal tissues and could be "achieve" due to the pH_e in tumor tissues.

The β-CD-NH_2 leaving studies of DOX@MSN-B-CD-PEG in PBS at pH 5.0 and 37 °C were taken through zeta-potential measurements as well. And the results are also shown in Fig. 4. The zeta-potential of DOX@MSN-B-CD-PEG at pH 5.0 decreased to − 2.01 mV within 0.5 h and kept decreasing to − 6.70 mV within 48 h. Broken down of the boronate ester revealed the phenylboronic acid groups of the carriers, leading to the negative zeta-potential of the nanoparticles. The results proved that β-CD-NH_2 could leaving the carriers at pH_i, which meant the carriers could "open the gate" to release the loaded drugs.

pH_i-dependent in vitro drug release studies

Firstly, to determine drug entrapment efficiency (EE) and the drug loading capacity (LC) of the drug carriers, DOX@MSN-B-CD-PEG was dissolved in HF solution. And the EE and LC of the nanoparticles were measured and calculated as 56.8 and 26.8%. The release amount of the loaded drug from the carriers at different pH values in buffer solution was measured by UV–Vis absorbing. As shown in Fig. 5, the accumulative DOX release amounts of DOX@MSN-B-CD-PEG at pH 7.4 were 16.6% within 24 h and 27.6% within 120 h, proved the pores of DOX@MSN-B-CD-PEG were effectively capped by β-CD-NH_2. Similar with that of pH 7.4, the drug release rate of the drug carriers at pH_e (6.5) was slow as well (the accumulative release amounts were 18.6% within 24 h and 29.5% within 120 h). The slow drug release rates at pH 7.4 and 6.5 proved that boronate ester bond linking MSNs and β-CD-NH_2 hydrolyzed little to prevent drug release at both pH values effectively.

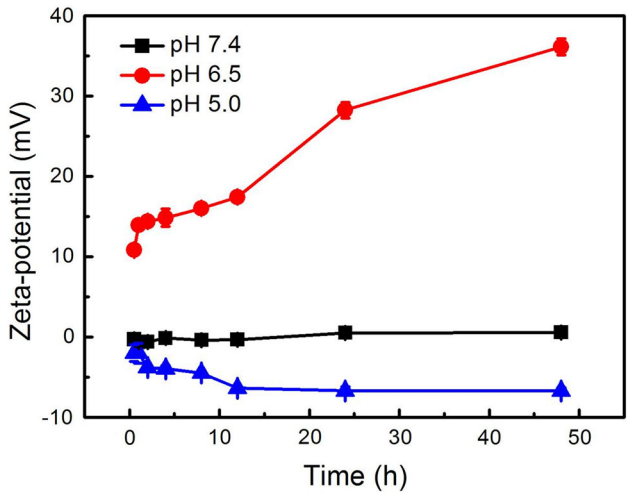

Figure 4 Zeta-potential changes of DOX@MSN-B-CD-PEG as a function of incubation time at pH 7.4, 6.5 and 5.0.

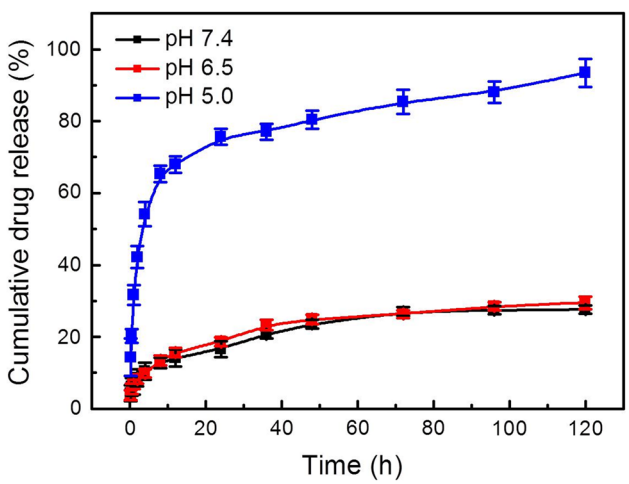

Figure 5 The controlled release profiles of DOX@MSN-B-CD-PEG at different pH values (7.4, 6.5 and 5.0).

Though the benzoic imine bonds linking the mPEG and β-CD-NH_2 could be interrupted at pH 6.5, the boronate ester was also steady. That could prevent the premature drug release before the carriers entering the cancer cells. At pH 5.0, the pH intracellular (pH_i), the drug release rates were accelerated obviously. The broken down of the boronate ester bonds leading to a rapid release of DOX at pH_i. The accumulative release amounts of DOX@MSN-B-CD-PEG at pH 5.0 were as high as 65.3% within 8 h, 80.4% within 48 h and 93.5% within 120 h. The results demonstrated that DOX@MSN-B-CD-PEG could encapsulate most of the drugs outside the cancer cells, but quickly release of the DOX intracellular.

pH_e-dependent in vitro cellular uptake studies

Due to the mPEG protective layer, DOX@MSN-B-CD-PEG should be "stealthy" and difficult cytophagy in bloodstream and normal tissues at pH 7.4. However, at pH 6.5, pH_e of tumor tissues, the hydrolysis of pH-sensitive benzoic imine bonds leading to the leaving of mPEG and revealing of positive-charged amino groups, which could enhance the cellular uptake of the drug carriers. Therefore, CLSM was applied to study the cellular uptake behavior of the nanoparticles in HeLa cell at pH 7.4 and 6.5, respectively. The CLSM images are shown in Fig. 6. After 4 h of *co*-incubation with DOX@MSN-B-CD-PEG at different pH values, HeLa cells showed different cellular uptake behavior of the nanoparticles. For pH 6.5, intensive red fluorescence of DOX present inside the cells (Fig. 6a–c); meanwhile, at pH 7.4, an evidently weaker red fluorescence could be detected (Fig. 6d–f). The difference in the fluorescence intensities indicated that the cellular uptake of DOX@MSN-B-CD-PEG at pH 6.5 was distinctly easier than that at pH 7.4, which demonstrated that drug carriers was "stealthy" at pH 7.4 but could be "activated" at pH_e.

Flow cytometry analyses were applied to quantitatively measure the cytophagy behavior of the carriers in HeLa cell at different pH values as well. As shown in Fig. 7, being consistent with the results of CLSM images, the cellular uptake amount of DOX@MSN-B-CD-PEG at pH 6.5 was distinctly higher than that at pH 7.4. The mean fluorescence

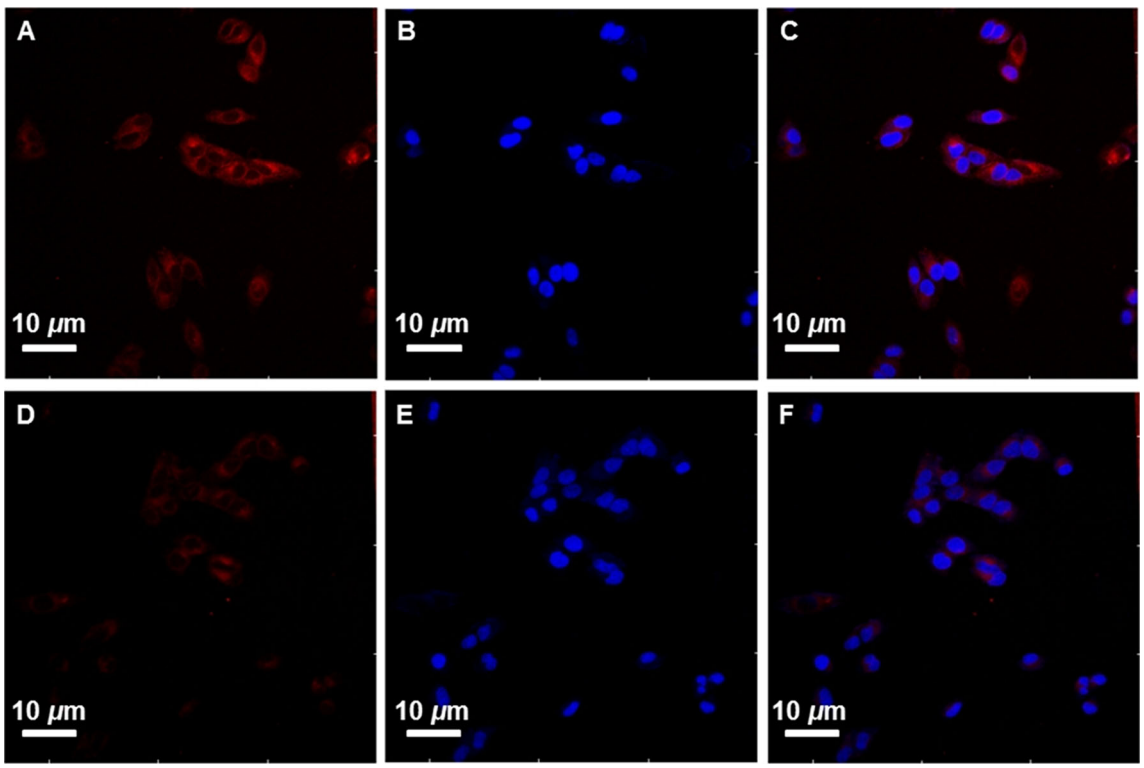

Figure 6 CLSM images of HeLa cells *co*-incubated with DOX@MSN-B-CD-PEG at different pH values: **a**, **d** red fluorescence excited from DOX, **b**, **e** blue fluorescence excited from DAPI indicating of nucleus and **c**, **f** an overall of red fluorescence and blue fluorescence. **a**–**c**: pH 6.5 and **d**–**f**: pH 7.4.

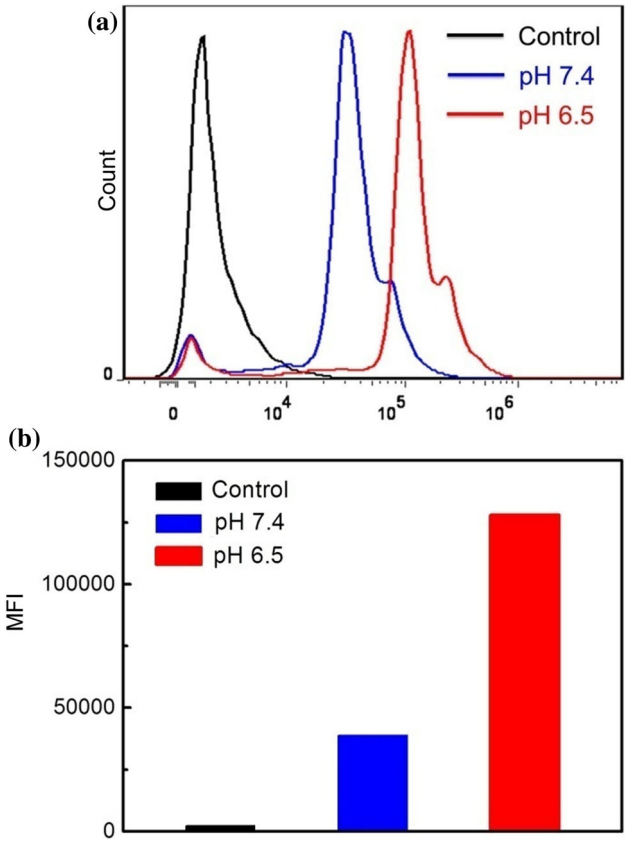

Figure 7 Flow cytometry analysis of HeLa cells *co*-incubated with DOX@MSN-B-CD-PEG at pH 6.5 (red) and pH 7.4 (blue) for 4 h. Blank was used as a control (black). The concentration of DOX was 2 mg/L.

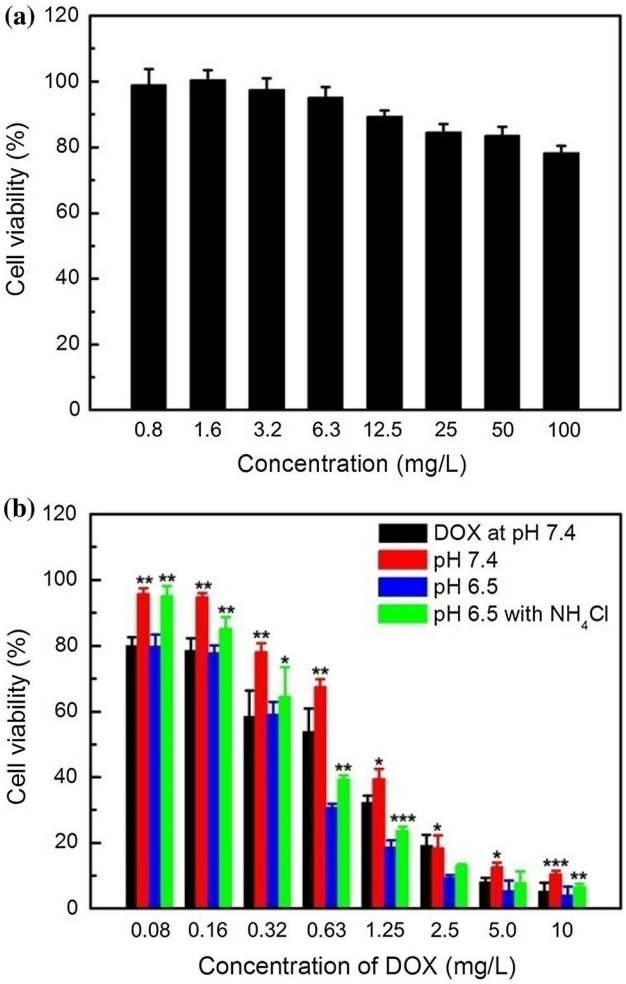

Figure 8 Cell viability of HeLa cells *co*-incubated with MSN-B-CD-PEG at pH 7.4 with different concentrations (**a**) and DOX@MSN-B-CD-PEG at pH 7.4, 6.5 and pH 6.5 with 20 mM NH_4Cl with different DOX concentrations, respectively (**b**). Statistical significance in differences was analyzed compared to the cell viability at pH 6.5 without NH_4Cl.

intensity (MFI) values at both pH values were also calculates, and the values at pH 6.5 were ~ 3.4 fold higher than that at pH 7.4. Combining with the CLSM images, the flow cytometry analyses results also proved that the mPEG protective layer could shield the nanoparticles against the cellular uptake in bloodstream and normal tissues at pH 7.4, and could leave the carriers to enhance whose ability of cellular uptake. In other words, the results proved the effect of the dynamic protection strategy.

In vitro cytotoxicity

For anti-cancer drug delivery, drug carriers should be safe and low biological toxicity; therefore, MTT assay was first applied to evaluate the cytocoxictiy of pure carriers MSN-B-CD-PEG without loading of DOX. As shown in Fig. 8a, the pure carriers exhibited a low cytotoxicity. The cell viability was ~ 90% at the concentration of MSN-B-CD-PEG 12.5 mg/L. With the concentration of the carriers rose to 100 mg/L, the cell viability was still higher than 78%. The results demonstrated that the pure MSN-B-CD-PEG without loading of DOX had a good cell biocompatibility.

MTT assay was also applied to investigate the in vitro anti-cancer ability of DOX loaded drug carriers DOX@MSN-B-CD-PEG. After being *co*-incubated with the carriers for 48 h at pH 7.4 and 6.5, respectively, the cell viabilities were significantly different at both pH values. The mPEG leaving studies and in vitro cellular uptake studies had proved that mPEG could be separated from the

carriers more easily at pH 6.5 than that at pH 7.4, and the cytophagy ability of the carriers by HeLa cells at pH 6.5 was evidently better than that at pH 7.4. The in vitro drug release studies also proved that the DOX release amounts at pH 7.4 and 6.5 were nearly the same. Therefore, undoubtedly, the cell viabilities at the same concentration of DOX at pH 7.4 were significantly higher than that at pH 6.5. It is shown in Fig. 8b, the cell viability of HeLa cells decreased with the increasing concentration of DOX. After being *co*-incubated with DOX@MSN-B-CD-PEG at pH 7.4 for 48 h, less than 12% of HeLa cells were killed at the DOX concentration of 0.32 mg/L. And the cell viabilities at the DOX concentrations of 1.25 and 10 mg/L were still ~ 40 and 10%, respectively, which were obviously higher than that of pure DOX (~ 59, 32 and 5.3%, respectively). By contrast, at pH 6.5, less than 60% cells were still alive at the DOX concentration of 0.32 mg/L; and the cell viabilities at the DOX concentrations of 1.25 mg/L and 10 mg/L were ~ 19 and 4.1%, respectively. The treatment effects DOX@MSN-B-CD-PEG at pH 6.5 were approach, or even better than that of pure DOX. The results demonstrated that the dynamic protection strategy could indeed reduce the side effects in normal tissues (pH_e ~ 7.4) without decreasing the treatment effects in tumor tissues (pH_e ~ 6.5).

To further evaluate the pH-sensitivity of the boronate ester bond intracellular, HeLa cells were pretreated with 20 mM NH_4Cl, which can trigger restoration of intracellular pH [33], and were then *co*-incubated with the carriers for 48 h at pH 6.5. Compared with that without being pretreated, the cell viability increased obviously. The cell viabilities at the DOX concentrations of 0.32, 1.25 and 10 mg/L were ~ 65, 24 and 6.5%, respectively, much higher than that without pretreatment. The pretreatment of HeLa cells with NH_4Cl can raise the pH intracellular [33], which could reduce the release rate of DOX from the drug carriers. Therefore, though DOX@MSN-B-CD-PEG could enter the cells at pH_e 6.5, fewer drugs could be released in the same time, leading to the increasing of the cell viability. Combining with the drug release studies, the results also demonstrated the dual-pH-sensitivity of DOX@MSN-B-CD-PEG as well as the tumor-triggered intracellular drug release property of the drug carriers.

Conclusions

In conclusion, a novel dual-pH-sensitive DDS with a tumor-triggered intracellular drug releasing property was developed. The DDS named DOX@MSN-B-CD-PEG was fabricated with a MSN core which loaded of model drug DOX, and with a dynamic mPEG protection layer which was coated on the surface of the drug carriers through a pH-sensitive benzoic imine bond. The benzoic imine bond was stable at pH 7.4; therefore, the carriers were protected by mPEG and were difficult cellular uptake in normal tissues. However, at pH 6.5, pH_e of tumor tissues, hydrolysis of the benzoic imine bond led to the leaving of mPEG and the revealing the positive charge of the carriers, which could enhance the cellular uptake ability of the carriers. The pores of MSN were capped by β-CD-NH_2 through another pH-sensitive boronate ester bond. After entering the cancer cells, due to the lower pH intracellular (pH_i), boronate ester bond was hydrolyzed and resulted in departure of β-CD-NH_2 and releasing DOX to kill the HeLa cells. With the dynamic protection strategy, the dual-pH-sensitive DOX@MSN-B-CD-PEG could improve the drug utilization in cancer cells effectively, and should be an excellent choice in cancer therapy fields.

Acknowledgements

This study was funded by National Natural Science Foundation of China (51773055 and 31401498) and Wuhan Morning Light Plan of Youth Science and Technology (2017050304010283).

Compliance with ethical standards

Conflict of interest The authors declare that they have no conflict of interest.

Electronic supplementary material: The online version of this article (https://doi.org/10.1007/s10853-018-2363-8) contains supplementary material, which is available to authorized users.

References

[1] Sun QH, Sun XR, Ma XP, Zhou ZX, Jin EL, Zhang B, Shen YQ, Van Kirk E A, Murdoch WJ, Lott JR, Lodge TP, Radosz

M, Zhao YL (2014) Integration of nanoassembly functions for an effective delivery cascade for cancer drugs. Adv Mater 26:7615–7621

[2] Sun QH, Zhou ZX, Qiu NS, Shen YQ (2017) Rational design of cancer nanomedicine: nanoproperty integration and synchronization. Adv Mater 29:1606628–1606646

[3] Shi J, Kantoff PW, Wooster R, Farokhzad OC (2017) Cancer nanomedicine: progress, challenges and opportunities. Nat Rev Cancer 17:20–37

[4] Dai L, Liu J, Luo Z, Li M, Cai K (2016) Tumor therapy: targeted drug delivery systems. J Mater Chem B 4:6758–6772

[5] Yang K, Feng L, Liu Z (2016) Stimuli responsive drug delivery systems based on nano-graphene for cancer therapy. Adv Drug Deliv Rev 105:228–241

[6] Luong D, Kesharwania P, Deshmukh R, Amin MCIM, Gupta U, Greish K, Iyer AK (2016) PEGylated PAMAM dendrimers: enhancing efficacy and mitigating toxicity for effective anticancer drug and gene delivery. Acta Biomater 43:14–29

[7] Yingchoncharoen P, Kalinowski DS, Richardson Des R (2016) Lipid-based drug delivery systems in cancer therapy: what is available and what is yet to come. Pharmacol Rev 68:701–787

[8] Al-Ahmady Z, Kostarelos K (2016) Chemical components for the design of temperature-responsive vesicles as cancer therapeutics. Chem Rev 116:3883–3918

[9] Bawa KK, Oh JK (2017) Stimulus-responsive degradable polylactide-based block copolymer nanoassemblies for controlled/enhanced drug delivery. Mol. Pharm 14:2460–2474

[10] Han L, Zhang XY, Wang YL, Li X, Yang XH, Huang M, Hu K, Li LH, Wei Y (2017) Redox-responsive theranostic nanoplatforms based on inorganic nanomaterials. J Control Release 259:40–52

[11] Llopis-Lorente A, Lozano-Torres B, Bernardos A, Martínez-Máñez R, Sancenón F (2017) Mesoporous silica materials for controlled delivery based on enzymes. J Mater Chem B 5:3069–3083

[12] Yu M, Gu Z, Ottewell T, Yu C (2017) Silica-based nanoparticles for therapeutic protein delivery. J Mater Chem B 5:3241–3252

[13] Wen J, Yang K, Liu F, Li H, Xu Y, Sun S (2017) Diverse gatekeepers for mesoporous silica nanoparticle based drug delivery systems. Chem Soc Rev 46:6024–6045

[14] Aznar E, Oroval M, Pascual L, Ramón Murguía J, Martínez-Máñez R, Sancenón F (2016) Gated materials for on-command release of guest molecules. Chem Rev 116:561–718

[15] de la Torre C, Agostini A, Mondragón L, Orzáez M, Sancenón F, Martínez-Máñez R, Marcos MD, Amorós P, Pérez-Payá E (2014) Temperature-controlled release by changes in the secondary structure of peptides anchored onto mesoporous silica supports. Chem Commun 50:3184–3186

[16] Chen H, Zheng D, Liu J, Kuang Y, Li Q, Zhang M, Ye H, Qin H, Xu Y, Li C, Jiang B (2016) pH-sensitive drug delivery system based on modified dextrin coated mesoporous silica nanoparticles. Int J Biol Macromol 85:596–603

[17] Hu JJ, Liu LH, Li ZY, Zhuo RX, Zhang XZ (2016) MMP-responsive theranostic nanoplatform based on mesoporous silica nanoparticles for tumor imaging and targeted drug delivery. J Mater Chem B 4:1932–1940

[18] Zhang M, Liu J, Kuang Y, Li Q, Chen H, Ye H, Guo L, Xu Y, Chen X, Li C, Jiang B (2016) "Stealthy" chitosan/mesoporous silica nanoparticle based complex system for tumor-triggered intracellular drug release. J Mater Chem B 4:3387–3397

[19] Martínez-Carmona M, Lozano D, Baeza A, Colilla M, Vallet-Regí M (2017) A novel visible light responsive nanosystem for cancer treatment. Nanoscale 9:15967–15973

[20] Tang Y, Hu H, Zhang MG, Song J, Nie L, Wang S, Niu G, Huang P, Lu G, Chen X (2015) An aptamer-targeting photoresponsive drug delivery system using "off–on" graphene oxide wrapped mesoporous silica nanoparticles. Nanoscale 7:6304–6310

[21] Paris JL, Cabañas MV, Manzano M, Vallet-Regí M (2015) Polymer-grafted mesoporous silica nanoparticles as ultrasound-responsive drug carriers. ACS Nano 9:11023–11033

[22] Nakamura T, Akita H, Yamada Y, Hatakeyama H, Harashima H (2012) A multifunctional envelope-type nanodevice for use in nanomedicine: concept and applications. Acc Chem Res 45:1113–1121

[23] Li W, Zhan P, De Clercq E, Lou H, Liu X (2013) Current drug research on PEGylation with small molecular agents. Prog Polym Sci 38:421–444

[24] Zhang J, Yuan ZF, Wang Y, Chen WH, Luo GF, Cheng SX, Zhuo RX, Zhang XZ (2013) Multifunctional envelope-type mesoporous silica nanoparticles for tumor-triggered targeting drug delivery. J Am Chem Soc 135:5068–5073

[25] Kunath K, Avon Harpe, Petersen H, Fischer D, Voigt K, Kissel T, Bickel U (2002) The structure of PEG-modified poly(ethylene imines) influences biodistribution and pharmacokinetics of their complexes with NF-kappaB decoy in mice. Pharm Res 19:810–817

[26] Zheng DW, Chen JL, Zhu JY, Rong L, Li B, Lei Q, Fan JX, Zou MZ, Li C, Cheng SX, Xu ZS, Zhang XZ (2016) Highly integrated nano-platform for breaking the barrier between chemotherapy and immunotherapy. Nano Lett 16:4341–4347

[27] Xin Y, Yuan J (2012) Schiff's base as a stimuli-responsive linker in polymer chemistry. Polym Chem 3:3045–3055

[28] Mo R, Gu Z (2016) Tumor microenvironment and intracellular signal-activated nanomaterials for anticancer drug delivery. Mater Today 19:274–283

[29] Quan CY, Chen JX, Wang HY, Li C, Chang C, Zhang XZ, Zhuo RX (2010) Core-shell nanosized assemblies mediated by the alpha-beta cyclodextrin dimer with a tumor-triggered targeting property. ACS Nano 4:4211–4219

[30] Kanamala M, Wilson WR, Yang M, Palmer BD, Wu Z (2016) Mechanisms and biomaterials in pH-responsive tumour targeted drug delivery: a review. Biomaterials 85:152–167

[31] Yang B, Jia HZ, Wang XL, Chen S, Zhang XZ, Zhuo RX, Feng J (2014) Self-assembled vehicle construction via boronic acid coupling and host-guest interaction for serum-tolerant DNA transport and pH-responsive drug delivery. Adv Healthcare Mater 4:596–608

[32] Li ZY, Hu JJ, Xu Q, Chen S, Jia HZ, Sun YX, Zhuo RX, Zhang XZ (2014) A redox-responsive drug delivery system based on RGD containing peptide-capped mesoporous silica nanoparticles. J Mater Chem B 3:39–44

[33] Luan J, Wu K, Li C, Liu J, Ni X, Xiao M, Xu Y, Kuang Y, Jiang F (2017) pH-sensitive drug delivery system based on hydrophobic modified konjac glucomannan. Carbohydr Polym 171:9–17